NANO LETTERS

Letter

pubs.acs.org/NanoLett

Plasmonic Nanoclocks

Hailong Liu,*[,†] Zilong Wang,[†] Jian Huang,[‡] Yan Jun Liu,[§] Hong Jin Fan,[†] Nikolay I. Zheludev,[†,∥] and Cesare Soci[†]

[†]Centre for Disruptive Photonic Technologies, Nanyang Technological University, Singapore, 637371

[‡]Department of Electrical and Computer Engineering, National University of Singapore, Singapore, 117576

[§]Institute of Materials Research and Engineering, Agency for Science, Technology and Research (A*STAR), 3 Research Link, Singapore, 117602

[∥]Optoelectronics Research Centre and Centre for Photonic Metamaterials, University of Southampton, Southampton SO17 1BJ, United Kingdom

S *Supporting Information*

ABSTRACT: Plasmonic spectra of "nanoclock" metamaterials can be topologically mapped on a torus. We manufactured arrays of such a metamaterial with different "time" shown on the clocks and demonstrated that the near-infrared spectra of the nanostructures can be predictably tuned exhibiting a rich series of high-order plasmon modes, from the electric dipole to exotic electric triakontadipole that could be engaged in chemo/biosensor applications.

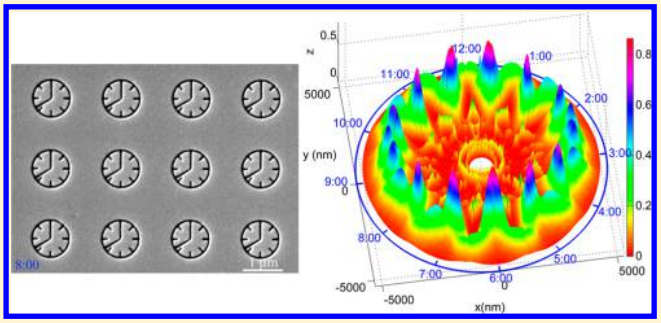

KEYWORDS: *Metamaterials, nanoclocks, high-order plasmon modes, topological map*

In metamaterials, the geometrical shape of their building blocks is the main "design parameter" that determines optical properties.[1−3] The design process is often determined by the intuitively driven exploration for new geometries. With the rapid development of nanofabrication technologies, various metamaterials consisting of different shapes and sizes of metamolecules have been proposed and fabricated to demonstrate unique optical properties,[4−9] hence enabling applications such as high-sensitivity biosensors,[10−13] surface-enhanced spectroscopy,[14−16] color filters,[17,18] and many other. Design of metamolecules underlying such applications usually relies on intuitive understanding of shape-optical mode relationship within geometrical shapes like metal rods, discs, split-ring resonators, antennas, chiral helices, nanoclusters, etc.[19−21] Based on plasmon hybridization models, the unique optical properties of metamaterials can be decomposed as the couplings of localized surface plasmon resonances (LSPRs) of the constituent building blocks (metamolecules).[22−26] LSPRs in metamolecules can be roughly categorized into the fundamental dipole mode and high-order resonant modes (quadrupole, octupole, hexadecapole, triakontadipole, etc.).[27−29] The fundamental dipole mode is a bright and superradiative mode that can be directly excited by normally incident light, while high-order plasmon modes are usually dark and subradiative modes, and are difficult to observe directly at normal incidence. However, high-order plasmon modes of a single nanoparticle can be excited by decreasing or breaking the symmetry[30−34] or can be coupled with low-order plasmon modes of other nanoparticles in its proximity,[35−39] if the nanoparticle to be excited supports high-order plasmon resonances.

Compared to dipole modes, high-order plasmon modes have lower radiative losses, higher quality factors, and sharper peaks,[37] which make them attractive for applications like biosensing and single molecule detection. So far quadrupole and octupole plasmon modes have been experimentally demonstrated in high-order nanostructures with complex shape such as "XI",[40] "ring/disk",[41−44] and "theta",[35] mostly relying on dipole-high-order plasmon couplings. However, superhigh-order plasmon modes, such as triakontadipole and even higher-order modes, have not yet been experimentally demonstrated. Indeed, the design of weakly resonant, high-order plasmonic modes in discrete nanostructures with a limited number of geometrical parameters is rather challenging. Here we introduce a new metamaterial with "nanoclock" metamolecule which appears to have unique and incredibly rich plasmonic properties: the "time" shown by the hour and minute hands of the nanoclock on metal dial is a single parameter variation which has a dramatic yet continuous effect on the optical response of the metamaterial array. To reveal the continuous and periodic nature of this combinatorial design paradigm we topologically map on a torus the "time" shown on

Received: May 28, 2014
Revised: July 29, 2014
Published: August 4, 2014

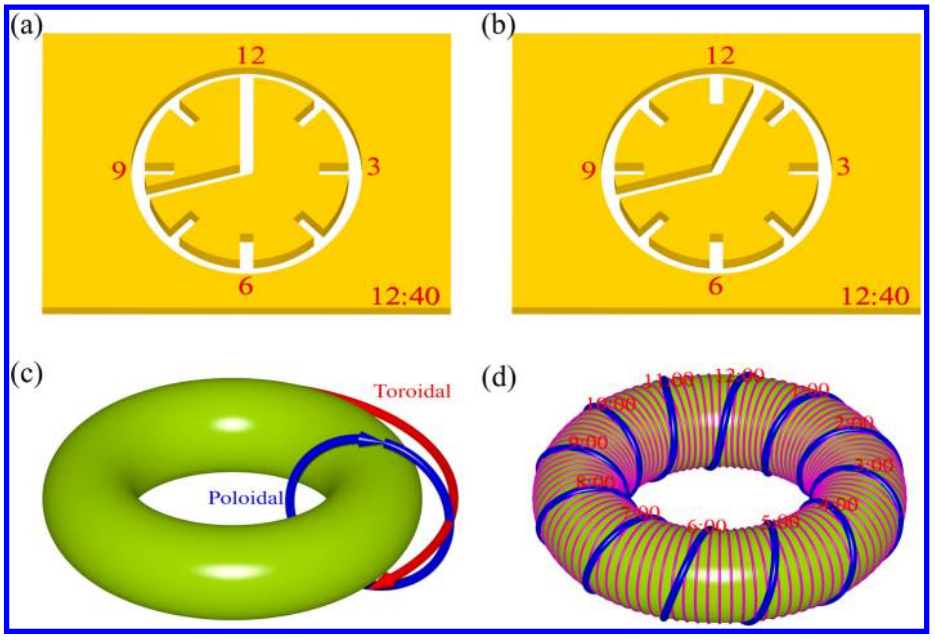

Figure 1. Schematic diagram of nanoclocks and nanoclock topology. (a) Fixed-hour nanoclock, in which the hour hand is fixed and the minute hand is rotated around the nanoclock face. Here, the hour hand is fixed at 12:00, and the minute hand is rotated to the position of 40 min. (b) 12-h analog nanoclock, in which both hands rotate synchronously around the face, in the 12:40 configuration. (c) Nanoclock topology: the set of all possible positions of the hour and minute hands of a clock is topologically equivalent to the surface of a torus, where the hour hand spans the toroidal direction (red arrow) and the minute hand the poloidal direction (blue arrow). (d) Fixed-hour versus 12-h analog nanoclock topology. In a fixed-hour nanoclock rotation of the minute hand corresponds to cross-sectional circles of the torus revolving around the toroidal direction (purple circles); in a 12-h analog nanoclock, the hour hand rotates synchronously with the minute hand, spanning 30° every full turn (360°) of the minute hand. This corresponds to the toroidal line on the surface of the torus (blue line).

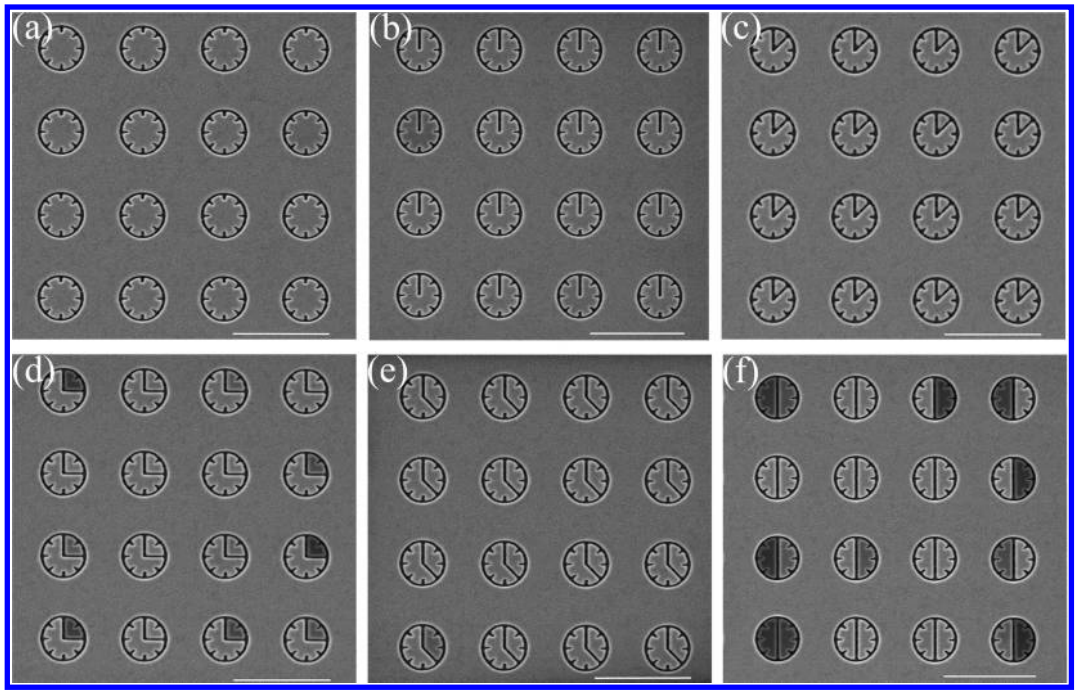

Figure 2. SEM images of the fabricated fixed-hour nanoclocks out of a thin film of gold: (a) nanoclock-face, (b) nanoclock-0°, (c) nanoclock-45°, (d) nanoclock-90°, (e) nanoclock-135°, and (f) nanoclock-180°. Scale bars: 2 μm.

the clock together with the corresponding optical spectra: upon change of "time" series of plasmonic resonances from the simple electric dipole to exotic electric 128-pole, and everything in between, are manifested. Using focused ion beam milling we manufactured in gold film metamaterial samples with different "time" shown on the clocks and confirmed that the near-infrared spectra of the nanostructures can be predictably tuned and high-order resonances observed. We argue that the nanoclock metamaterial is a useful platform in the design of frequency selective surfaces and polarization sensitive devices. Moreover, the analytical potential of plasmonic sensors can be

dx.doi.org/10.1021/nl501997z | *Nano Lett.* 2014, 14, 5162−5169

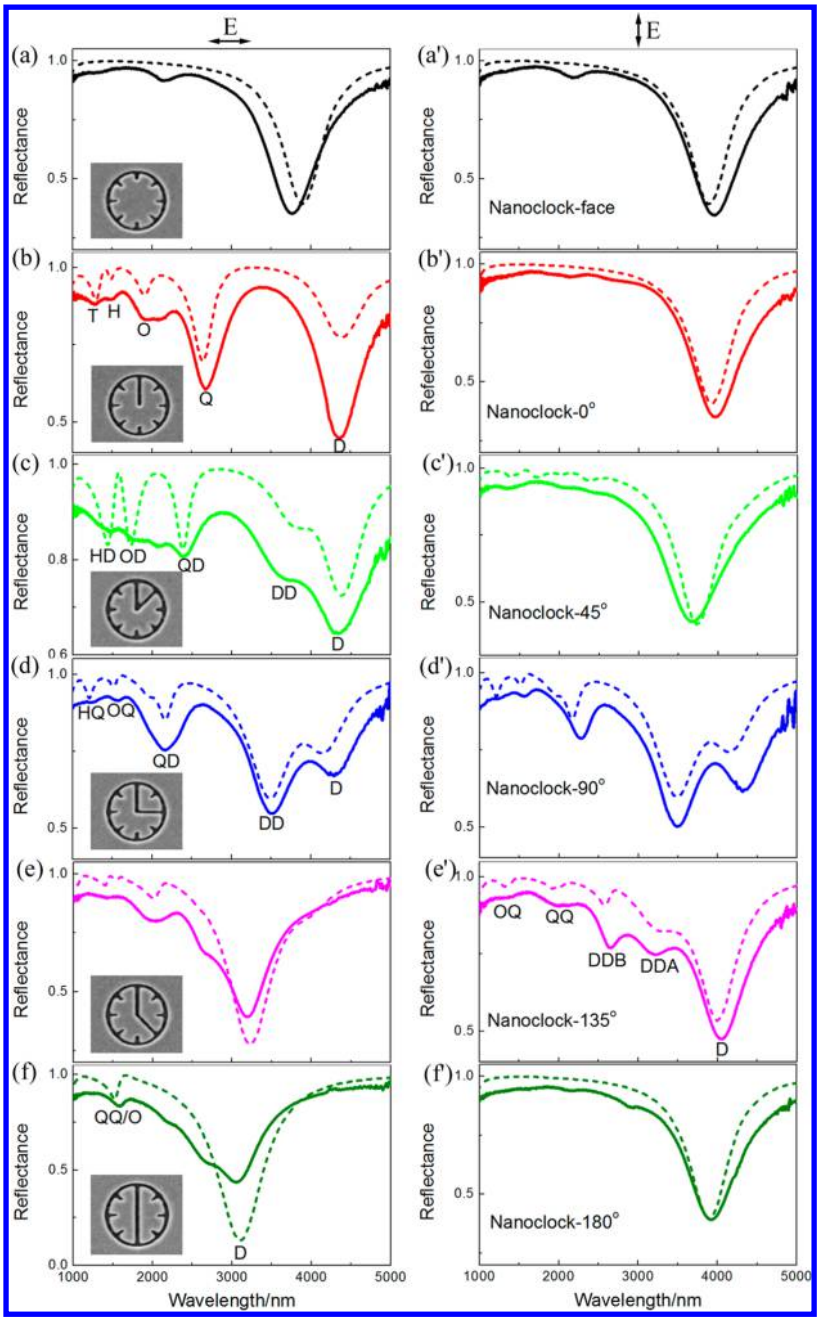

Figure 3. Nanoclock plasmonic resonances in the near-infrared spectral region. Reflectance spectra of nanoclocks in the case of horizontal (left column) and vertical (right column) incident light polarizations. Solid lines represent measured spectra, while dashed lines are simulation results.

considerably extended with nanoclock nanostructures by giving access to high-order plasmonic resonances.

Figure 1 shows schematic diagrams of the proposed nanoclocks and their equivalent topology. A nanoclock unit is composed of a nanoclock-face and two hands that represent the hours and the minutes (Figure 1a and b). The nanoclock-face consists of an annular aperture enclosing a central gold disc with eight symmetric markers repeated every 45°. Note that, for symmetry reasons and ease of fabrication, here we employed a design with 8 markers instead of 12 as in conventional analog clocks. For any given face, the hour and the minute hand positions can be tuned continuously and independently. All their possible positions are topologically equivalent to the surface of a torus (Figure 1c), where the hour hand spans the toroidal direction (red arrow), while the minute hand follows the poloidal direction (blue arrow). These two degrees of freedom span a large parameter space, giving rise to rich combinations of plasmonic resonances within the spectral range from visible to far-infrared, mainly depending on the size of the nanoclock-face.

To confine the parameter space of our study, we considered two types of nanoclocks, the "fixed-hour nanoclock" (Figure 1a) and the "12-hour analog nanoclock" (Figure 1b). The *fixed-hour nanoclock* has a single degree of freedom, where the hour hand position is fixed while the minute hand rotates around the nanoclock-face. Figure 1a shows the specific 12:40 configuration of a fixed-hour nanoclock, in which the hour hand is fixed along the vertical direction (12:00) and the minute hand is rotated to the position corresponding to 40 min. As the hour hand is kept at a fixed position, the set of all possible positions

dx.doi.org/10.1021/nl501997z | *Nano Lett.* 2014, 14, 5162−5169

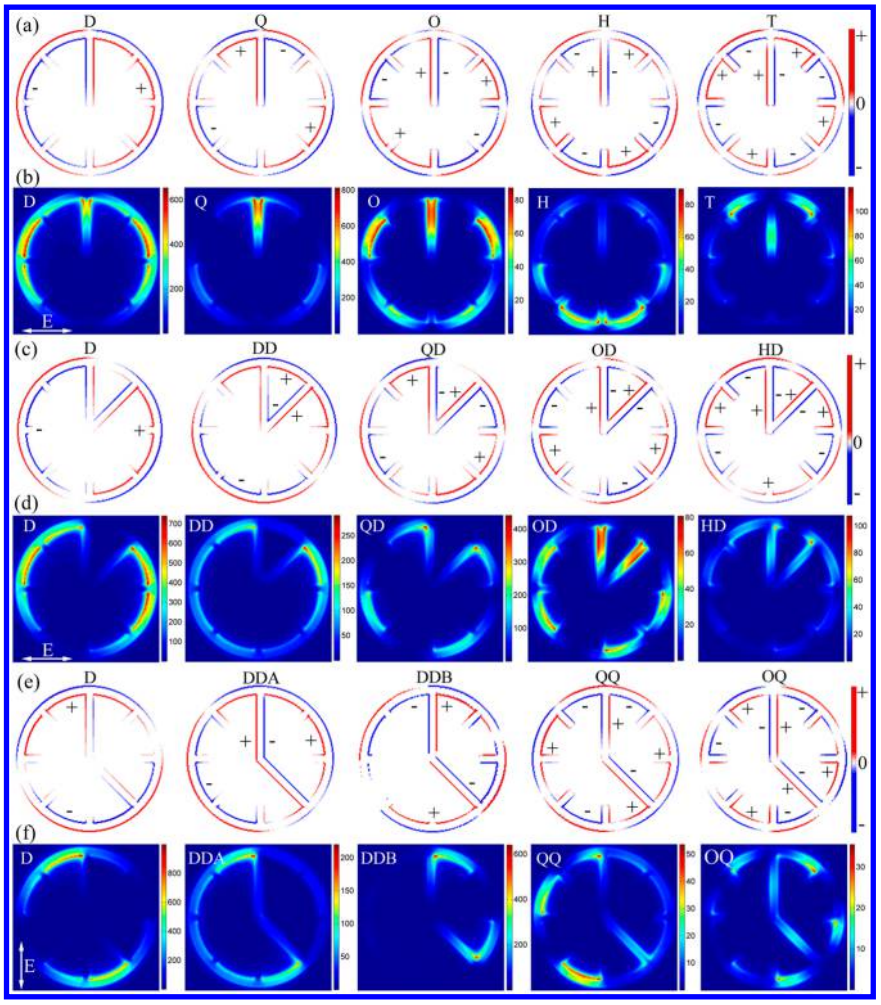

Figure 4. Representative charge (a, c, e) and electric field (b, d, f) distributions of fixed-hour nanoclocks: nanoclock-0° (a–b) and nanoclock-45° (c–d) with horizontal polarization; nanoclock-135° (e–f) with vertical polarization.

of the minute hand is topologically equivalent to cross-sectional circles of the torus revolving around the toroidal direction (purple circles in Figure 1d). The *12-h analog nanoclock* has two degrees of freedom, where the hour hand rotates synchronously with the minute hand spanning 30° every full turn (360°) of the minute hand, like in conventional clocks. Figure 1b shows the 12:40 configuration of a 12-h analog nanoclock. In this case, positions of hour and minute hands are mutually dependent, and their movement maps onto a toroidal line on the surface of the torus (blue line in Figure 1d). In the following, we first discuss experimental investigation of plasmonic resonances of fixed-hour nanoclocks and then present a comprehensive study on combinatorial design of 12-h analog plasmonic nanoclocks.

To investigate the optical properties of fixed-hour nanoclocks, we fabricated a series of nanoclocks on a gold film using focused ion beam milling. To prepare the gold film, a titanium adhesion layer (3 nm) and a gold layer (120 nm) were subsequently deposited onto a quartz substrate by electron beam evaporation. Each nanoclock array has an area of 30 × 30 μm^2, and the pitch between nanoclocks is 1.7 μm in both dimensions. Figure 2 shows scanning electron microscope (SEM) images of the fabricated nanoclocks. Figure 2a is a bare nanoclock-face array, which contains no hands. In Figure 2b–f, the hour hand is fixed along the vertical direction (12:00), while the minute hand is rotated clockwise. Based on the angle between these two hands, the fabricated nanoclocks in Figure 2b–f are termed as nanoclock-0°, 45°, 90°, 135°, and 180°, respectively. The dark regions in Figure 2d and f are caused by the charging effect in the SEM scanning process. Nominal design parameters for these nanoclocks are the following: the inner and outer radii of the annular aperture are r = 420 nm and R = 475 nm; the length and width of the markers are l = 120 nm and w = 55 nm; the length and width of the hands are 420 and 55 nm, respectively.

Figure 3 shows the measured and simulated reflectance spectra of the fixed-hour nanoclocks in Figure 2. Optical properties were characterized by a Fourier-transform infrared spectrometer (Bruker Vertex 80v) equipped with a confocal microscope (Hyperion 1000). A 36× Cassegrain objective with numerical aperture of 0.5 is used in our microscope. For numerical simulations, a commercial finite-difference time-domain software (Lumerical FDTD Solutions) is used to calculate the reflectance spectra and the corresponding near-field distributions. Overall, the simulated spectra (dash lines) agree well with the experimental results (solid lines) in Figure 3. The presented fixed-hour nanoclocks show polarization-dependent spectral profiles, except for the case of nanoclock-face.

Plasmonic Mode Analysis of the Fixed-Hour Nanoclocks. For the sake of discussion, we classify the optical responses of plasmonic nanoclocks (Figure 3) into four categories: (I) dipolar plasmon modes, (II) high-order plasmon

dx.doi.org/10.1021/nl501997z | *Nano Lett.* 2014, 14, 5162–5169

modes, (III) dipolar and high-order plasmon coupling modes, and (IV) high-order and high-order plasmon coupling modes. Note that there are two kinds of dipolar plasmon modes, and their nature is different. Interestingly, these two types of dipole modes can be simultaneously observed in nanoclock-45°, 90°, and 135° with horizontal or vertical polarization, changing the incident polarization into two directions.

I. Dipolar Plasmon Modes. The bare nanoclock-face shows a single broad resonant dip in reflectance spectra (Figure 3a and a′). The discrepancy in the small resonances around 2200 nm between measured and simulated spectra in Figure 3a and a′ may be affected by the nonperfect homology of the small markers and the small *k*-vector spread of the Cassegrain objective. The calculated electric-field and charge distributions (see Figure S1 in the Supporting Information) of the broad resonant dip show that this dip originates from the surface plasmon polariton mode of the milled nanoholes consisting of annular aperture and markers. This effect is similar to the band-pass filtering of typical annular apertures, in which the resonant modes is ascribed to the coupling of localized guided mode and the distributed surface plasmon polaritions.[45,46] The charge distribution (see Supporting Information, Figure S1) illustrates its dipolar nature. To distinguish this dipole mode from dipole−dipole modes discussed in the following, we refer to this resonant mode as fundamental dipole mode. All of the fixed-hour nanoclocks show a fundamental dipolar mode (the resonant peak with the longest resonant wavelength in each spectrum) due to the band-pass filtering effect of nanoclock-face and the hour and minute hands. The inserted hour and minute hands will shift the fundamental dipolar modes, as shown in Figure 3b−f′.

In nanoclocks-45°, 90°, and 135°, there is an additional kind of dipolar mode (marked by DD or DDA), as shown in Figure 3c−e′. For nanoclock-45°, the electric-field distributions (see Figure 4d) and the corresponding spectra simulation results (not shown here) demonstrate that this kind of dipolar peak originates from the dipolar−dipolar plasmonic coupling mode between the two sectorial nanoparticles. An interesting observation is that dips DD and D are both dipolar modes, but their charge density and electric-field distributions are not aligned to the polarization of incident light (horizontal direction). They are converted into two directions. By rotating the polarization of incident light with 10° very step, the polarized eigenmodes of dips DD and D emerge around −20° and 70°, respectively, with respect to the horizontal direction (see Figure S2 in the Supporting Information). Therefore, we observe two dipolar resonant peaks with two different polarization states, which can be used as frequency selective surfaces. Similar polarization conversion has been previously observed in planar "S" and "L" shaped nanoholes.[47,48] To realize a larger rotational angle than 45°, multilayer structures and increasing film thickness have been employed for these patterns.[48] Conversely, in our nanoclock-45°, the rotation angle of peak DD for nanoclock-45° is about 70° without changing the film thickness, and it can be gradually tuned to a near-complete 90° by varying the hand angle. Note that nanoclock-0° and 180° do not show polarization conversion for horizontal (P0) and vertical (P90) polarizations, which is due to their symmetrical geometry shapes in these two polarizations. However, nanoclock-0° and 180° have polarization converting effects with incident polarization deviating from horizontal (P0) or vertical direction (P90), and we will discuss it in the polarization effect part.

II. High-Order Plasmon Modes. In addition to shifting the fundamental dipolar modes and converting polarizations, insertion of the hands induces high-order plasmon modes. In case of nanoclock-0°, the two completely overlapping hands break the symmetry and make high-order plasmon resonances easily excited with horizontal light polarization. The eight markers in the nanoclock face effectively increase the circumference of central disc, which shifts multipole modes to infrared regions. Therefore, in nanoclock-0° one can observe the emergence of a series of high-order modes, like the four resonant dips labeled by Q, O, H, and T in Figure 3b. To reveal their origin, the corresponding near-field charge and electric-field distributions were calculated and shown in Figure 4a and b. Here the central disc has 4, 6, 8, and 10 charge nodes at dips Q, O, H, and T; thus we assign these dips to quadrupolar (Q), octupolar (O), hexadecapolar (H), and triakontadipolar (T) plasmonic modes, respectively. Due to the limitation of our measurement setup, we simulated the optical response of nanoclock-0° within 500 and 1000 nm (see Figure S3(a) in the Supporting Information). Even higher resonant modes, 64-pole (hexacontatetrapole, marked by HT) and 128-pole (marked by HTE), are observed in nanoclock-0° within this optical region (see Figure S3a and S4 in the Supporting Information). The high quality factors of triakontadipole and 128-pole of nanoclock-0° make them quite desirable for improving the figure of merit of plasmonic sensors. Moreover, a magnetic plasmonic mode is observed in nanoclock-0° within the visible optical region, marked by M in Figure S3a (see the Supporting Information). This magnetic response mainly originates from the displacement current between the two closely sides of the vertical hand (see the Supporting Information Figure S4c), which is similar to the magnetic mode of the split nanoball.[49]

III. Dipolar and High-Order Plasmon Coupling Modes. As the angle between the hour and the minute hands increases, the central disc is divided into two nanosectors. The plasmonic modes of these two nanosectors couple and form new resonant modes. In nanoclock-45°, simulations show that the dipolar resonant wavelength of the small nanosector is close to that of the high-order resonant modes of the large nanosector, so that they may couple and hybridize to form high-order resonant dips (QD, OD, and HD) in reflectance spectra (Figure 3c). The corresponding charge and electric-field distributions, shown in Figure 4c and d, indicate that the dipole mode of the small nanosector couples with quadrupole, octupole, and hexadecapole modes of the large nanosector and forms the dips of HD (hexadecapole−dipole coupling), OD (octupole−dipole coupling), and QD (quadrupole−dipole coupling), respectively. Triakontadipole−dipole (TD) coupling mode can be observed within 500 and 1000 nm (see Figure S3b in the Supporting Information). In nanoclock-90° there is also a quadrupole−dipole coupling mode (marked by QD in Figure 3d). A similar dipolar and high-order plasmon coupling was shown in ring/disk nanostructures.[28,44]

IV. High-Order and High-Order Plasmon Couplings. Due to the symmetry of design, optical response of nanoclock-90° is equivalent for vertical and horizontal polarizations (Figures 3d and d′). When the hand angle is increased from 45° to 90°, the size of the small nanosector increases and the corresponding resonance peaks are red-shifted, while the size of the large nanosector decreases and its resonance peaks are blue-shifted. As a result, the quadrupole mode of the small nanosector approaches the octupole and hexadecapole modes of the large nanosector. Therefore, these modes couple and hybridize to

dx.doi.org/10.1021/nl501997z | Nano Lett. 2014, 14, 5162−5169

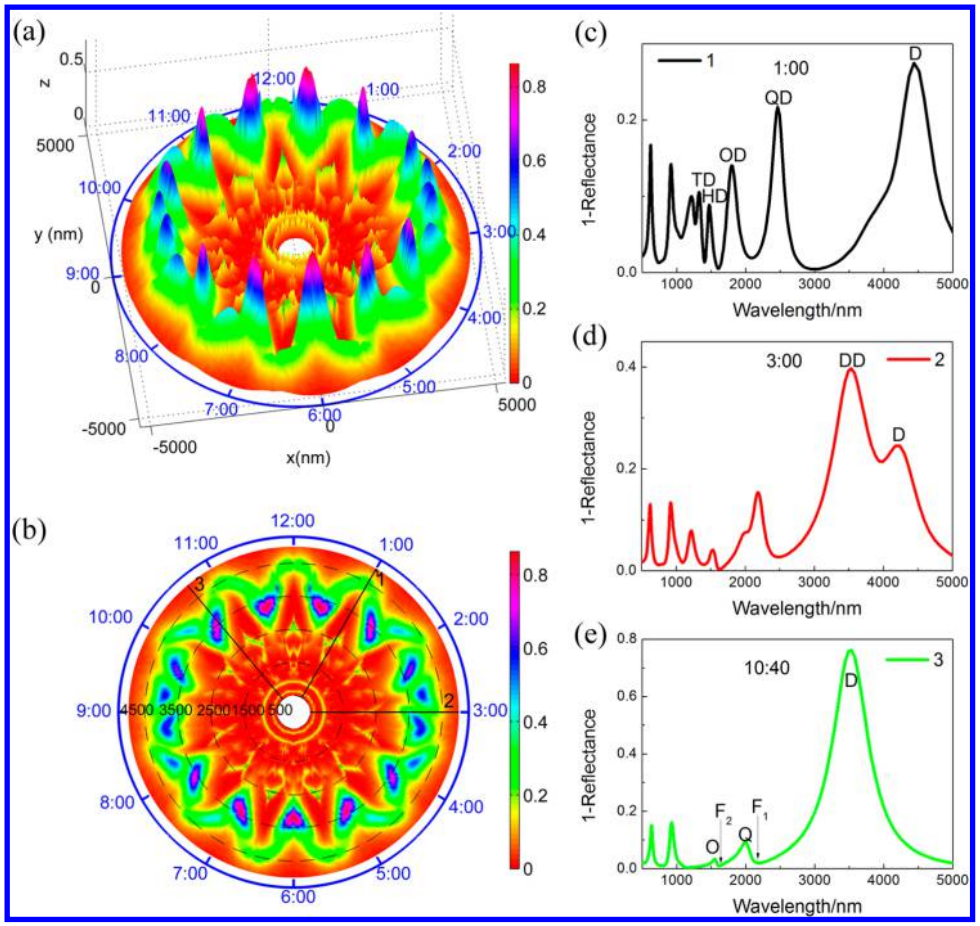

Figure 5. Parametric mapping of plasmonic modes of 12-h analog nanoclocks. (a) 3D map in cylindrical coordinates: the radial distance represents resonant wavelength, the azimuthal angle corresponds to nanoclock time (hour and minute hand configuration), while the vertical height shows the resonant amplitude (1 − reflectance). (b) 2D contour map (dashed contour lines correspond to different wavelengths). Strong optical resonances appear at different times (cut-out lines 1−3): (c−e) are the corresponding 1:00, 3:00, and 10:40 spectra, illustrating the appearance of high-order modes, polarization rotations, and Fano resonances (F).

form the hexadecapole−quadrupole (HQ) and octupole−quadrupole (OQ) plasmon coupling modes seen in the reflectance spectrum of nanoclock-90°. The charge distributions for dips OQ and HQ in nanoclock-90° (see Figure S5 in the Supporting Information) confirm their nature of high-order and high-order plasmon coupling modes, which are different from dips OD and HD (octupole−dipole plasmon coupling, hexadecapole−dipole plasmon coupling) in nanoclock-45°.

When the hand angle reaches 135°, the two nanosectors have a comparable size, and high-order with high-order plasmon couplings are also observed in nanoclock-135°. In Figure 3e′, the two coupled dips indicated by QQ and OQ stem from plasmon coupling of quadrupole−quadrupole and octupole-quadrupole modes, respectively. The charge distributions in Figure 4e and f illustrate their nature of high-order and high-order plasmon couplings. As we continually increase the hand angle to 180°, the two nanosectors become of identical size, and their resonant modes coincide. In Figure 2f, the dip indicated by QQ/O is a quadrupole−quadrupole plasmon coupling mode, since the corresponding charge distributions (see Figure S6 of the Supporting Information) show that both nanosectors oscillate in quadrupole modes. If we combine the two equal nanosectors as a whole unit, the nanoclock is oscillating in an octupolar mode.

As discussed above, the optical response of fixed-hour nanoclocks is polarization-dependent. In addition to the horizontal and vertical polarization, we theoretically investigate the optical response of nanoclocks to different polarizations (see Figure S7 in the Supporting Information). For dipolar plasmon modes, nanoclocks have the strongest resonant intensity with light polarization parallel or perpendicular to the bisector of the angle between two hands, which can be explained by the symmetric and antisymmetric modes of the "V-shaped" nanoparticle.[50] Most importantly, we can directly determine the polarization angle for each high-order mode with the strongest resonant intensity in Figure S7 (see the Supporting Information), which provides an additional degree of freedom in the design of nanoclocks. Film thickness is another important parameter influencing the resonant modes of nanoclocks. We select nanoclock-0° and 45° as examples to show the influence of film thickness on the resonant modes (see the Supporting Information, Figure S3). With increasing the film thickness, the resonant intensities of resonant modes decrease, while the quality factors increase. To reach a compromise between resonant intensity and quality factor, we select 120 nm as the thickness of gold film.

Parametric Analysis of Plasmonic Modes in 12-h Analog Nanoclocks. Thus far, we investigated the influence of a single hand rotation on the plasmon modes of nanoclocks. As two hands are allowed to rotate around their cross point, richer optical features arise. We have conducted combinatorial investigation[51] of plasmonic multipole modes and their

dx.doi.org/10.1021/nl501997z | Nano Lett. 2014, 14, 5162−5169

couplings in 12-h analog nanoclocks within the parameter space described by the blue toroidal line in Figure 1d. The simulated results for fixed horizontal polarization are displayed in Figure 5. To characterize the "time" dependence and strength of the resonant modes of nanoclocks, we first plot the optical response of nanoclocks in a cylindrical coordinate system, as shown in Figure 5a. In this three-dimensional map, the radial distance defines the resonant wavelength (from 500 to 5000 nm), the azimuthal angular coordinate represents the nanoclock time (the configuration of hour and minute hands), and the vertical height (z) indicates the amplitude of 1 − reflectance. The corresponding 2D contour map of the resonant modes is shown in Figure 5b. The maps in Figure 5a and b are 2-fold symmetric along the y-axis. The corresponding 2-fold symmetric configurations of nanoclocks are the complementary times whose sum is 12:00, such as 2:40 and 9:20. This is because the relative positions of the two hands for any pair of complementary times are identical with respect to horizontal polarization. The peripheral peaks correspond to dipole modes of nanoclocks including the fundamental dipolar modes and the dipole−dipole coupling modes. The innermost ring corresponds to the magnetic plasmonic mode of nanoclocks. Between the innermost ring and the peripheral peaks there are many plasmonic resonances, which derive from the combinatorial effects of high-order plasmon modes of nanoclocks with different hand configurations. Parametric mapping provides a complete visualization of plasmonic modes supported by nanoclocks, from which one can theoretically predict the fundamental relations between the "time" displaying on the array of gold nanoclock dials and multipole plasmonic resonances. Strong optical resonances appear around "of the clock" and "half an hour" times, which would make them the option of choice for high-sensitivity chemo/biosensors and other specialized applications. The spectra of "times" 12:00, 1:00, and 3:30, etc. illustrate the appearance of strong resonant high-order modes. At 1:00 (Figure 5c and line 1 in Figure 5b), the resonant peaks QD, OD, HD, and TD result from the couplings between high-order modes and the dipole mode. At times around 2:00, 3:00, 3:30, and so forth, two dipolar modes exist simultaneously, which results in polarization rotation. This is the case of the two dipolar modes (D and DD) in the spectrum at 3:00 (Figure 5d and line 2 in Figure 5b). Moreover, with appropriate parameters, high-order modes can also overlap and form high-order Fano resonances. Figure 5e gives example of nanoclock 10:40 (line 3 in Figure 5b), which displays two high-order Fano resonances (F_1 and F_2) formed by the overlap of octupole, quadrupole, and dipole modes.

In summary, we experimentally and theoretically established the fundamental relations between the "time" displaying on the array of nanoclock dials and multipole plasmonic resonances of the array. The rich optical features of nanoclocks are ascribed to the combination of band-pass filtering effects of milled nanoholes and plasmon couplings and hybridizations of nanosectors. Magnetic plasmon mode, polarization conversions, and high-order Fano resonances are all shown in nanoclocks. Combinatorial mapping of plasmonic modes of nanoclocks within the topologically equivalent toroidal space of parameters that describe hour and minute hand configurations is presented. This work paves a way for implementing plasmonic devices, such as polarization filters or chemo/biosensors, where "analog" design parameters of a constant set of functional plasmonic molecules can be tuned at will to achieve the desired optical response.

■ ASSOCIATED CONTENT

Supporting Information

Charge, electric field distributions of nanoclock-face, 90°, and 180°; charge, electric field, and magnetic field distributions of 64-pole, 128-pole, and magnetic mode in nanoclock-0°; influence of polarization and film thickness on plasmonic modes of nanoclocks. This material is available free of charge via the Internet at http://pubs.acs.org.

■ AUTHOR INFORMATION

Corresponding Author

*E-mail: liuhl@ntu.edu.sg.

Notes

The authors declare no competing financial interest.

■ ACKNOWLEDGMENTS

The authors thank Dr. Vassili Savinov and Dr. Si Guangyuan for their fruitful discussion. This work is supported by the Ministry of Education of Singapore (Grant No. MOE2011-T3-1-005), the NTU-NAP startup grant No. M4080511. H.J.F. appreciates the funding support from MOE Tier 1 grant (RG 66/11).

■ REFERENCES

(1) Wang, H.; Brandl, D. W.; Nordlander, P.; Halas, N. J. *Acc. Chem. Res.* **2007**, *40*, 53−62.
(2) Barro, S. J.; Wei, X.; Baldauf, J. S.; Funston, A. M.; Mulvaney, P. *Nat. Commun.* **2012**, *3*, 1275.
(3) Staude, I.; Decker, M.; Ventura, M. J.; Jagadish, C.; Neshev, D. N.; Gu, M.; Kivshar, Y. S. *Adv. Mater.* **2013**, *25*, 1260−1264.
(4) Luk'yanchuk, B.; Zheludev, N. I.; Maier, S. A.; Halas, N. J.; Nordlander, P.; Giessen, H.; Chong, C. T. *Nat. Mater.* **2010**, *9*, 707−715.
(5) Hentschel, M.; Saliba, M.; Vogelgesang, R.; Giessen, H.; Alivisatos, A. P.; Liu, N. *Nano Lett.* **2010**, *10*, 2721−2726.
(6) Verellen, N.; Sonnefraud, Y.; Sobhani, H.; Hao, F.; Moshchalkov, V. V.; Van Dorpe, P.; Nordlander, P.; Maier, S. A. *Nano Lett.* **2009**, *9*, 1663−1667.
(7) Liu, H.; Leong, E. S. P.; Wang, Z.; Si, G.; Zheng, L.; Liu, Y. J.; Soci, C. *Adv. Opt. Mater.* **2013**, *1*, 978−983.
(8) Liu, N.; Weiss, T.; Mesch, M.; Langguth, L.; Eigenthaler, U.; Hirscher, M.; Sönnichsen, C.; Giessen, H. *Nano Lett.* **2010**, *10*, 1103−1107.
(9) Cetin, A. E.; Artar, A.; Turkmen, M.; Yanik, A. A.; Altug, H. *Opt. Express* **2011**, *19*, 22607−22618.
(10) Mayer, K. M.; Hafner, J. H. *Chem. Rev.* **2011**, *111*, 3828−3857.
(11) Lal, S.; Link, S.; Halas, N. J. *Nat. Photonics* **2007**, *1*, 641−648.
(12) Acimovic, S. S.; Kreuzer, M. P.; Gonzalez, M. U.; Quidant, R. *ACS Nano* **2009**, *3*, 1231−1237.
(13) Zhao, J.; Zhang, C.; Braun, P. V.; Giessen, H. *Adv. Mater.* **2012**, *24*, OP247−OP252.
(14) Tanaka, K.; Plum, E.; Ou, J. Y.; Uchino, T.; Zheludev, N. I. *Phys. Rev. Lett.* **2010**, *105*, 227403.
(15) Giannini, V.; Vecchi, G.; Gómez Rivas, J. *Phys. Rev. Lett.* **2010**, *105*, 266801.
(16) Talley, C. E.; Jackson, J. B.; Oubre, C.; Grady, N. K.; Hollars, C. W.; Lane, S. M.; Huser, T. R.; Nordlander, P.; Halas, N. J. *Nano Lett.* **2005**, *5*, 1569−1574.
(17) Xu, T.; Wu, Y.; Luo, X.; Guo, L. J. *Nat. Commun.* **2010**, *1*, 59.
(18) Liu, Y. J.; Si, G. Y.; Leong, P. E. S.; Xiang, N.; Danner, A. J.; Teng, J. H. *Adv. Mater.* **2012**, *24*, OP131−OP135.

(19) Knight, M. W.; Liu, L.; Wang, Y.; Brown, L.; Mukherjee, S.; King, N. S.; Everitt, H. O.; Nordlander, P.; Halas, N. J. *Nano Lett.* **2012**, *12*, 6000−6004.
(20) Ou, J. Y.; Plum, E.; Jiang, L.; Zheludev, N. I. *Nano Lett.* **2011**, *11*, 2142−2144.
(21) Schreiber, R.; Luong, N.; Fan, Z.; Kuzyk, A.; Nickels, P. C.; Zhang, T.; Smith, D. M.; Yurke, B.; Kuang, W.; Govorov, A. O.; Lied, T. *Nat. Commun.* **2013**, *4*, 2948.
(22) Prodan, E.; Radloff, C.; Halas, N. J.; Nordlander, P. *Science* **2003**, *302*, 419−422.
(23) Funston, A. M.; Novo, C.; Davis, T. J.; Mulvaney, P. *Nano Lett.* **2009**, *9*, 1651−1658.
(24) Ye, J.; Lagae, L.; Maes, G.; Gorghs, G.; Van Dorpe, P. *Opt. Express* **2009**, *17*, 23765−23771.
(25) Liu, H.; Wu, X.; Li, B.; Xu, C.; Zhang, G.; Zheng, L. *Appl. Phys. Lett.* **2012**, *100*, 153114.
(26) Liu, H.; Li, B.; Zheng, L.; Xu, C.; Zhang, G.; Wu, X.; Xiang, N. *Opt. Lett.* **2013**, *38*, 977−979.
(27) Langhammer, C.; Schwind, M.; Kasemo, B.; Zoric, I. *Nano Lett.* **2008**, *8*, 1461−1471.
(28) Fu, Y. H.; Zhang, J. B.; Yu, Y. F.; Luk'yanchuk, B. *ACS Nano* **2012**, *6*, 5130−5137.
(29) Hao, F.; Larsson, E. M.; Ali, T. A.; Sutherland, D. S.; Nordlander, P. *Chem. Phys. Lett.* **2008**, *458*, 262−266.
(30) Mukherjee, S.; Sobhani, H.; Lassiter, J. B.; Bardhan, R.; Nordlander, P.; Halas, N. J. *Nano Lett.* **2010**, *10*, 2694−2701.
(31) Fang, Z.; Cai, J.; Yan, Z.; Nordlander, P.; Halas, N. J.; Zhu, X. *Nano Lett.* **2011**, *11*, 4475−4479.
(32) Ye, J.; Verellen, N.; Van Roy, W.; Lagae, L.; Maes, G.; Borghs, G.; Van Dorpe, P. *ACS Nano* **2010**, *4*, 1457−1464.
(33) Liu, S. D.; Zhang, Z. S.; Wang, Q. Q. *Opt. Express* **2009**, *17*, 2906−2917.
(34) Cai, Y.; Li, Y.; Nordlander, P.; Cremer, P. S. *Nano Lett.* **2012**, *12*, 4881−4888.
(35) Habteyes, T. G.; Dhuey, S.; Cabrini, S.; Schuck, P. J.; Leone, S. R. *Nano Lett.* **2011**, *11*, 1819−1825.
(36) Brown, L. V.; Sobhani, H.; Lassiter, J. B.; Nordlander, P.; Halas, N. J. *ACS Nano* **2010**, *4*, 819−832.
(37) Verellen, N.; Van Dorpe, P.; Vercruysse, D.; Vandenbosch, G. A. E.; Moshchalkov, V. V. *Opt. Express* **2011**, *19*, 11034−11051.
(38) Hao, F.; Nordlander, P. *Phys. Rev. B* **2007**, *76*, 245417.
(39) Shao, L.; Fang, C.; Chen, H.; Man, Y. C.; Wang, J.; Lin, H. *Nano Lett.* **2012**, *12*, 1424−1430.
(40) Verellen, N.; Van Dorpe, P.; Huang, C.; Lodewijks, K.; Vandenbosch, G. A. E.; Lagae, L.; Moshchalkov, V. V. *Nano Lett.* **2011**, *11*, 391−397.
(41) Hao, F.; Nordlander, P.; Sonnefraud, Y.; Van Dorpe, P.; Maier, S. A. *ACS Nano* **2009**, *3*, 643−652.
(42) Sonnefraud, Y.; Verellen, N.; Sobhani, H.; Vandenbosch, G. A. E.; Moshchalkov, V. V.; Van Dorpe, P.; Nordlander, P.; Maier, S. A. *ACS Nano* **2010**, *4*, 1664−1670.
(43) Cetin, A. E.; Altug, H. *ACS Nano* **2012**, *6*, 9989−9995.
(44) Verellen, N.; Sonnefraud, Y.; Sobhani, H.; Hao, F.; Moshchalkov, V. V.; Van Dorpe, P.; Nordlander, P.; Maier, S. A. *Nano Lett.* **2009**, *9*, 1663−1667.
(45) Fan, W.; Zhang, S.; Minhas, B.; Malloy, J. K.; Brueck, S. R. J. *Phys. Rev. Lett.* **2005**, *94*, 033902.
(46) Krug, P. A.; Dawes, D. H.; McPhedran, R. C.; Wright, W.; Macfarlane, J. C.; Whitbourn, L. B. *Opt. Lett.* **1989**, *14*, 931−933.
(47) Wu, S.; Zhang, Z.; Zhang, Y.; Zhang, K.; Zhou, L.; Zhang, X.; Zhu, Y. *Phys. Rev. Lett.* **2013**, *110*, 207401.
(48) Li, T.; Liu, H.; Wang, S. M.; Yin, X. G.; Wang, F. M.; Zhu, S. N.; Zhang, X. *Appl. Phys. Lett.* **2008**, *93*, 021110.
(49) Kuznetsov, A. I.; Miroshnichenko, A. E.; Fu, Y. H.; Viswanathan, V.; Rahmani, M.; Valuckas, V.; Pan, Z. Y.; Kivshar, Y.; Pickard, D. S.; Luk'yanchuk, B. *Nat. Commun.* **2014**, *5*, 3104.
(50) Yu, N. F.; Genevet, P.; Kats, M. A.; Aieta, F.; Tetienne, J.; Capasso, F.; Gaburro, Z. *Science* **2011**, *334*, 333−337.
(51) Plum, E.; Tanaka, K.; Chen, W. T.; Fedotov, V. A.; Tsai, D. P.; Zheludev, N. I. *J. Opt.* **2011**, *13*, 055102.